Journal of Physics D: Applied Physics

PAPER

Assessment of large critical electric field in ultra-wide bandgap *p*-type spinel $ZnGa_2O_4$

To cite this article: Zeyu Chi *et al* 2023 *J. Phys. D: Appl. Phys.* **56** 105102

View the article online for updates and enhancements.

You may also like

- Enhancement in Cathodoluminescent Properties of Carbon Nanotube- $ZnGa_2O_4$: Mn^{2+} Phosphor Composites
J. H. Park, B. W. Park, N. S. Choi et al.
- A study for the influences of temperatures on $ZnGa_2O_4$ films and solar-blind sensing performances
Chengling Lu, Qingyi Zhang, Shan Li et al.
- Pulsed laser deposition of $ZnGa_2O_4$ thin films on Al_2O_3 and Si substrates for deep optoelectronic devices applications
Anqi Guo, Lichun Zhang, Ning Cao et al.

This content was downloaded from IP address 90.127.27.147 on 26/02/2023 at 14:53

J. Phys. D: Appl. Phys. 56 (2023) 105102 (7pp) https://doi.org/10.1088/1361-6463/acbb14

Assessment of large critical electric field in ultra-wide bandgap *p*-type spinel $ZnGa_2O_4$

Zeyu Chi[1], Tamar Tchelidze[2], Corinne Sartel[1], Tsotne Gamsakhurdashvili[2], Ismail Madaci[1], Hayate Yamano[3], Vincent Sallet[1], Yves Dumont[1], Amador Pérez-Tomás[5], Farid Medjdoub[4] and Ekaterine Chikoidze[1,*]

[1] Groupe d'Etude de la Matière Condensée (GEMaC), Université Paris-Saclay, UVSQ—CNRS, 45 Av. des Etats-Unis, 78035 Versailles Cedex, France
[2] Faculty of Exact and Natural Science, Department of Physics, Ivane Javakhishvili Tbilisi State University, 3 Av. Tchavtchavadze, 0179 Tbilisi, Georgia
[3] Department for Integrated Sensor Systems, Danube University Krems, 3500 Krems, Austria
[4] IEMN, CNRS, UMR8520, Av. Poincare, 59650 Villeneuve D'Ascq, France
[5] Catalan Institute of Nanoscience and Nanotechnology (ICN2), CSIC and The Barcelona Institute of Science and Technology, Barcelona, Spain

E-mail: ekaterine.chikoidze@uvsq.fr

Received 10 October 2022, revised 3 February 2023
Accepted for publication 10 February 2023
Published 22 February 2023

Abstract

The spinel zinc gallate $ZnGa_2O_4$ stands out among the emerging ultra-wide bandgap (∼5 eV) semiconductors as the ternary complex oxide with the widest gap where bipolar conductivity has been demonstrated. For power and energy electronics, a fundamental property of the material is its critical electric field (E_{CR}) although, for $ZnGa_2O_4$, is yet unknown. In this work, highly resistive *p*-type $ZnGa_2O_4$ thin films on sapphire and Si substrates were grown by metal organic chemical vapor deposition to determine both, the remote acceptor concentration and vertical breakdown voltage. Hall Effect measurements confirmed a low carrier concentration at room temperature of $\sim 10^{11}$ cm^{-3}. From vertical metal-semiconductor-metal structures the average E_{CR} has been estimated to be of at least 5.3 MV cm^{-1}, which already is significantly larger than the one of SiC and GaN.

Keywords: ultra-wide band gap, $ZnGa_2O_4$, electrical properties, critical electric field

(Some figures may appear in colour only in the online journal)

1. Introduction

Ultra-wide bandgap (UWBG) semiconductor oxides have recently attracted significant attention as a novel platform for ultra-high power electronics and deep ultraviolet opto-electronics [1]. The spinel zinc gallate ($ZnGa_2O_4$) stands out within the family of oxide UWBG ($E_g \sim 5$ eV) as an advanced semiconductor platform for applications such as photonics (i.e. photodetector [2], phototransistors [3–5], gas sensors [6], thin-film-transistors [7–9], or optical memory application [10]), thus, heralding novel spinel electronics. Spinel oxides have, indeed, a peculiar chemical formula AB_2O_4, where A and B cations occupy octahedral and tetrahedral sites formed by oxygen atoms. Thus, spinel oxides obey different doping rules from traditional binary semiconductor oxides because of their multivalent elements and different sites, such as the antisite defects due to the inverted distribution of cations [11].

* Author to whom any correspondence should be addressed.

 © 2023 IOP Publishing Ltd

The disordered distribution of ions and vacancies in the material, (caused by the so-called self-doping effect), can lead to intrinsic electron or hole conductivity [12].

Consequently, a wide range of intrinsic conductivities have been reported for $ZnGa_2O_4$. The resistivity of native n-$ZnGa_2O_4$ can be as low as 2.7×10^{-2} Ω·cm at room temperature (e.g. [7, 13]), while intrinsic p-$ZnGa_2O_4$ is, in general, rather insulating at room temperature. Indeed, Chikoidze *et al* [14] reported native p-type $ZnGa_2O_4$ thin films grown by metal organic chemical vapor deposition (MOCVD), where the intrinsic hole conductivity at high temperature was attributed to the antisite defects ZnGa. Therefore, the intrinsic conductivity of $ZnGa_2O_4$ thin films can be controlled well over ten orders of magnitude by tuning the growth conditions (cation ratio, oxygen pressure, etc) thanks to this self-doping effect [15]. In agreement with these empirical observations, Sabino *et al* [16] suggested by *ab-initio* simulations that both, n- and p-type conductivities could be achieved in $ZnGa_2O_4$, and the hole conductivity is likely achieved by a polaronic band due to excess of Zn. It should be noted, however, that the electronic and opto-electronic devices based on $ZnGa_2O_4$, are mostly unipolar (i.e. n-type) (e.g. [17]) and studies on p-type $ZnGa_2O_4$ devices are still very limited. However, to exploit the full potential of $ZnGa_2O_4$ spinel electronics, bipolar devices (such as p-n junction (photo) diodes, PiN rectifiers, lateral and vertical power MOSFETs) and p-type conductivity should be achieved.

The critical electric field (E_{CR}) of a material is a crucial parameter for assessing a semiconductor material's potential as a platform for power and energy electronics applications. In particular, the Baliga's figure of merit [18] is informative of the on-state/blocking device performance for power switching applications which primarily depends on carrier mobility and the cube of the critical electric field. Representative values of the critical electric field for the most common power electronics semiconductors, such as silicon (0.3 MV cm^{-1}), 4H-SiC (3.5 MV cm^{-1}) [19], GaN (3.9 MV cm^{-1}) [20], or AlGaN (5.9 MV cm^{-1} [21]) are well known. For other UWBG such as AlN, the E_{CR} values have also been reported (12 MV cm^{-1} [22]) while a generally agreed theoretical value for diamond is 10 MV cm^{-1} [23]. For β-Ga_2O_3, a common estimation for the upper limit given in the literature is $\sim$8 MV cm^{-1} [24], while this value may be well underestimated as it has recently been experimentally observed to be at least 8.32 MV cm^{-1} and 13.2 MV cm^{-1} for p-NiO/β-Ga_2O_3 junctions [25] and Zn-doped β-Ga_2O_3 [26], respectively. However, to the best of our knowledge, critical electric field values for $ZnGa_2O_4$ are not yet known.

Therefore, the objective of the present work was to define $ZnGa_2O_4$ thin films onto insulating and conducting substrates for assessing the remote concentration and to stablish a preliminary value of the $ZnGa_2O_4$ critical electric field, respectively. According to the kinetic impact ionization theory and previous studies on Ga_2O_3 [26], to achieve large critical electric fields, it is mandatory to obtain a sample with low remote carrier concentration to reduce the onset of the impact ionization process. In the present work, we studied $ZnGa_2O_4$ thin films, which are highly resistive p-type in nature due to their deep acceptor native defects as we will show further on.

2. Experimental details

$ZnGa_2O_4$ thin film were grown in a radio-frequency (RF) heated horizontal MOCVD reactor with separate inlets to avoid premature reactions in the manifold between oxygen and organometallics precursors. Trimethylgallium (TMGa), diethylzinc (DEZn) and, 5.5 N pure oxygen were used as gallium, zinc, and oxygen sources, respectively. The TMGa and DEZn bubbler temperatures were fixed at -10 °C and 0 °C, respectively. During the growth, the flow rates of TMGa, DEZn, and oxygen were kept at 11 μmol min^{-1}, 7 μmol min^{-1}, and 1200 sccm, respectively. The growth temperature and the reactor pressure were set at 775 °C, and 38 torr, respectively. The growth time was 90 min. Argon was used as carrier gas. To analyse the $ZnGa_2O_4$ crystal phases, x-ray diffraction profiles were recorded in θ/2θ configuration between 15° and 115°, using a Rigaku SmartLab apparatus equipped with a Cu-Kα source ($\lambda = 0.1541$ nm). The thicknesses of the thin films were determined by means of scanning electron microscopy (SEM) cross-sectional images from a JEOL JSM 7001 F scanning electron microscope.

For Hall effect measurements, Ohmic contacts were prepared with silver paint at the four corners of the sample. The resistivity and Hall effect measurements were performed, in a Van der Pauw configuration with perpendicularly to current applied magnetic fields varying from 0 to 1.6 T, in 550–850 K temperature range. The majority charge carrier sign, concentration, and mobility were then determined. A Keysight B1505A Power Device Analyzer has been used to carry out the vertical breakdown voltage measurements at room temperature. Negative bias has been applied on an isolated Ohmic contact with the grounded substrate to access the breakdown voltage.

3. Results and discussion

3.1. Thermodynamic analysis of point defects and free carriers

We conducted a thermodynamic analysis of point defects and free carriers for equilibrium condition to establish the optimal growth parameters of the $ZnGa_2O_4$ close to the stoichiometry composition. This thermodynamic analysis is carried out for the $ZnGa_2O_4$ (crystal)—O_2 (gas) system. It is a three-component two-phase system. Thus, according to Gibbs' phase rule, its degree of freedom is 3, so three thermodynamic parameters can vary freely. All material properties, including defects, free carriers' concentrations, and conductivity, depend on them. We chose the following independent variables: temperature T, oxygen partial pressure P_{O_2}, and the ratio of gallium and zinc partial pressures $x = \frac{P_{Ga}}{P_{Zn}}$.

To find the dependence of concentrations of defects and free carriers on these parameters we used the Kroger method of

quasi-chemical reactions [27]. Special attention is paid to discern if the concentration of antisite defects Ga_{Zn} and Zn_{Ga} can be controlled in such a way to impact *n*- and *p*-type conductivities. The processes we considered with the corresponding mass action law are the following:

The creation of a Schottky defect pairs:

$$\phi \leftrightarrows 2V_{Ga} + 3V_O,\ K_{S1} = [V_{Ga}]^2[V_O]^3 \tag{1}$$

$$\phi \leftrightarrows V_{Zn} + V_O,\ K_{S2} = [V_{Zn}][V_O] \tag{2}$$

where V_{Zn}, V_{Ga}, and V_O are zinc, gallium, and oxygen vacancies, respectively; $[V_{Zn}]$, $[V_{Ga}]$, and $[V_O]$ are their concentrations, respectively. The incorporation of oxygen atoms in a crystal from the surrounding atmosphere, when zinc and gallium vacancies are created:

$$\tfrac{1}{2}O_2 \leftrightarrows O_O + V_{Zn},\ K_{V_{Zn}} = \frac{[V_{Zn}]}{P_{O_2}^{1/2}} \tag{3}$$

$$\tfrac{3}{2}O_2 \leftrightarrows 3O_O + 2V_{Ga},\ K_{V_{Ga}} = \frac{[V_{Ga}]^2}{P_{O_2}^{3/2}}\ . \tag{4}$$

The lattice thermal ionization:

$$\phi \leftrightarrows e + h,\ K_i = np \tag{5}$$

where e and h are electrons and holes, respectively; n and p are their concentrations, respectively. The ionization of zinc, gallium and oxygen vacancies:

$$V_{Zn} \leftrightarrows V'_{Zn} + h,\ K_{iZn} = \frac{[V'_{Zn}]p}{[V_{Zn}]} \tag{6}$$

$$V_{Ga} \leftrightarrows V'_{Ga} + h,\ K_{iGa} = \frac{[V'_{Ga}]p}{[V_{Ga}]} \tag{7}$$

where V'_{Zn} and V'_{Ga} denote positively single-charged zinc and gallium vacancies, respectively; $[V'_{Zn}]$ and $[V'_{Ga}]$ are their concentrations, respectively. The ionization of oxygen vacancy:

$$V_O^{\bullet} \leftrightarrows V_O + e,\ K_{iO} = \frac{[V_O^{\bullet}]n}{[V_O]} \tag{8}$$

where $V_O^{\bullet}$ denotes negatively single-charged oxygen vacancy; $[V_O^{\bullet}]$ is its concentration. Creation of antisite defects via incorporation of metal atoms from the gas phase into vacancies:

$$Zn(g) + V_{Ga} \leftrightarrows Zn_{Ga},\ K_{Zn} = \frac{[Zn_{Ga}]}{[V_{Ga}]P_{Zn}} \tag{9}$$

$$Ga(g) + V_{Zn} \leftrightarrows Zn_{Ga},\ K_{Ga} = \frac{[Ga_{Zn}]}{[V_{Zn}]P_{Ga}} \tag{10}$$

where Zn_{Ga} and Ga_{Zn} are zinc in gallium site and gallium in zinc site anti-site defects, respectively; $[Zn_{Ga}]$ and $[Ga_{Zn}]$ are their concentrations, respectively. And their ionizations:

$$Zn_{Ga} \leftrightarrows Zn'_{Ga} + h,\ K_{iZn_{Ga}} = \frac{[Zn'_{Ga}]p}{[Zn_{Ga}]} \tag{11}$$

$$Ga_{Zn} \leftrightarrows Ga_{Zn}^{\bullet} + e,\ K_{iGa_{Zn}} = \frac{[Ga_{Zn}^{\bullet}]n}{[Ga_{Zn}]} \tag{12}$$

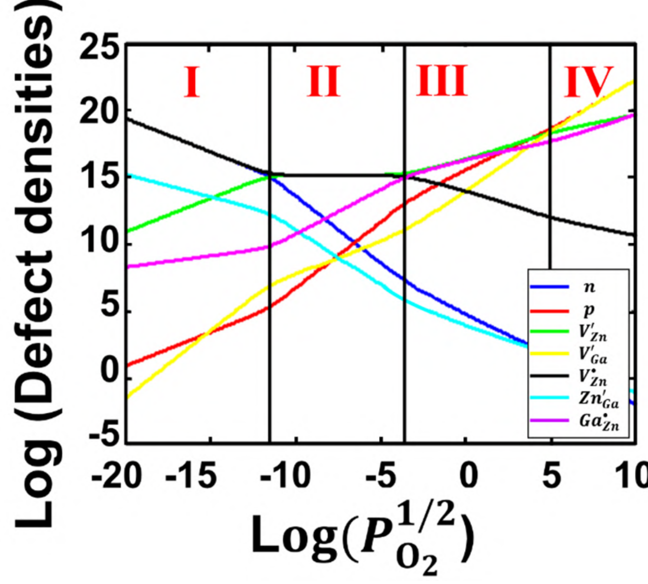

Figure 1. The dependence of concentration of point defects and free carriers on oxygen partial pressure, for $T = 775$ °C, and $x = \frac{P_{Ga}}{P_{Zn}} = 3$.

where Zn'_{Ga} and $Ga_{Zn}^{\bullet}$ are positively and negatively single-charged anti-site defects, respectively; $[Zn'_{Ga}]$ and $[Ga_{Zn}^{\bullet}]$ their concentrations, respectively. To find the concentration of defects and free carriers by the system of equations (1)–(12), the charge neutrality condition must be added:

$$n + [V'_{Zn}] + [V'_{Ga}] + [Zn'_{Ga}] \leftrightarrows p + [V_O^{\bullet}] + [Ga_{Zn}^{\bullet}]\ . \tag{13}$$

The connection between zinc, gallium, and oxygen partial pressures are defined by means of the constant of the zinc gallate creation reaction:

$$Zn(g) + 2Ga(g) + 2O_2(g) \leftrightarrows ZnGa_2O_4(s),\ K = P_{Zn}P_{Ga}^2P_{O_2}^2\ . \tag{14}$$

Having solved the system of equations (1)–(14), one can find the concentrations of defects and free carriers versus temperature, partial pressure of one component and ratio of gallium and zinc pressures. The calculated concentrations of charged defects and free carriers in dependence of oxygen partial pressure are shown in figure 1. The temperature was chosen to be 775 °C, the ratio $x = \frac{P_{Ga}}{P_{Zn}}$ equals to 3. These parameters correspond to our actual growth conditions. The $x = P_{Ga}/P_{Zn}$ ratio is roughly estimated on the base of TMGa and DEZn flow rates and their formation enthalpies:

$$x = \frac{P_{Ga}}{P_{Zn}} = \frac{J_{Ga}\sqrt{2m_{Ga}kT}\exp(-\Delta H_{Ga}/kT)}{J_{Zn}\sqrt{2m_{Zn}kT}\exp(-\Delta H_{Zn}/kT)}.$$

Here J_{Ga} and J_{Zn} are flow rates of TMGa and DEZn, respectively, m_{Ga} and m_{Zn} masses of Ga and Zn atoms, ΔH_{Ga} and ΔH_{Zn} formation enthalpies of TMGa and DEZn.

One can distinguish the following regions in the figure that:

(a) The region of intrinsic n-conductivity, origin of which are oxygen vacancies V_O. In this region $[V_O^\bullet] = n$, and they are dominant;
(b) The first region of self-compensation, here oxygen vacancies $[V_O^\bullet]$ and zinc vacancies $[V'_{Zn}]$ are dominant spices and $[V_O^\bullet] = [V'_{Zn}]$;
(c) The second region of self-compensation where zinc vacancies $[V'_{Zn}]$ and gallium in zinc sites $[Ga_{Zn}^\bullet]$ are dominant, and $[V'_{Zn}]=[Ga_{Zn}^\bullet]$. In this region, the concentration of holes exceeds the concentration of electrons significantly. Around $P_{O_2} = 1$ atm, the concentration of holes achieves 10^{15} cm^{-3}. It is remarkable that the concentration of holes at a whole range of pressure tails negatively charged gallium vacancies $[V'_{Ga}]$—the concentrations of V'_{Ga} and holes change the same way when oxygen partial pressure changes and difference between these concentrations is quite small along the whole pressure range.
(d) The region of hole conductivity, here $[V'_{Ga}]$ and holes are dominant spices. However, the oxygen pressure is unrealistically high here.

Notably, there is a very weak dependence of concentrations of free carriers on x. For $x = 10^{-3}$, that is, when the partial pressure of Zn exceeds the partial pressure of Ga three orders of magnitude, the concentration of holes increases only ten times, compared to $x = 3$.

Therefore, the growth of both n- and p-type $ZnGa_2O_4$ thin films are feasible by tuning the growth parameters such as, mainly oxygen partial pressure and temperature. The cations concentration ratio weakly affects the conductivity (as experimentally observed [14]). In this work, we concentrate on the regions predicted to correspond to p-type conductivity. Then, the highly-resistive p-type $ZnGa_2O_4$ thin layer was grown in the conditions which are input from thermodynamic analysis.

3.2. $ZnGa_2O_4$ thin film growth and structural properties

$ZnGa_2O_4$ thin films were grown on two kinds of substrates simultaneously: on conducting p-type Si(111) and c-oriented sapphire Al_2O_3(0001) (insulating) substrates. $ZnGa_2O_4$/Si sample was used to fabricate vertical parallel plane capacitors, and characterized vertically for breakdown voltage capability. While the $ZnGa_2O_4$/sapphire thin film was used for the investigation of the electrical transport properties (resistivity, carrier, mobility) at elevated temperatures in a Van Der Pauw configuration.

Figure 2 shows the Cu-Kα x-ray diffraction (XRD) spectra of $ZnGa_2O_4$ thin films grown on Si(111) and Al_2O_3(0001). According to the PDF 28–1240 file, it is pure $ZnGa_2O_4$ spinel without a secondary phase. Film on Si(111) is polycrystalline without any preferential texturization, similar to XRD pattern reported by Galazka *et al* [28] for their melt-grown bulk $ZnGa_2O_4$ spinel, milled in a randomly oriented

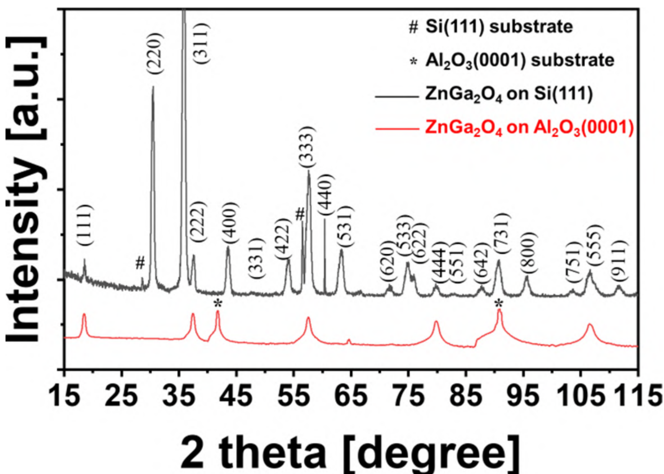

Figure 2. Cu-Kα XRD spectra of $ZnGa_2O_4$ thin film grown on Si(111) (black), and Al_2O_3(0001) (red). * and # correspond respectively to Al_2O_3(0001) and Si(111) Bragg reflections.

powder. For films on Al_2O_3(0001) substrates, Bragg peaks appearing at 18.6°, 37.6°, 57.6°, 79.7°, and 106.6° correspond to the (111), (222), (333), (444), and (555) planes of the cubic spinel $ZnGa_2O_4$, respectively, as reported by previous literature [14, 29].

$ZnGa_2O_4$ thin films have already been grown polycrystalline on sapphire substrates by MOCVD [30], RF magnetron sputtering [31, 32], pulsed laser deposition (PLD) [13], with a preferential orientation along [111] of cubic spinel and equivalent direction for Al_2O_3(0001). Analogously, $ZnGa_2O_4$ thin films have also been grown on Si substrates by atomic layer deposition (ALD) [29], PLD [33], and RF magnetron sputtering [32]. A larger lattice mismatch between $ZnGa_2O_4$ and Si(100) (which may also contain a native ultra-thin SiO_2 interlayer) results in a relatively weaker orientation of crystallite in the $ZnGa_2O_4$ grown on Si substrate than that on sapphire (0001) [32]. The full width at half maximum values were measured as 0.29° and 0.49° for $ZnGa_2O_4$ (111) on sapphire and Si(100) substrates, respectively, indicating also a smaller size of crystallites in the case of Si(111) substrates with respect to Al_2O_3(0001) ones.

3.3. Electrical transport properties

Hall and electrical transport properties were studied for $ZnGa_2O_4$ grown on Al_2O_3 crystals, as the sapphire substrate is insulating up to high temperatures thus preventing parasitic leakage through the substrate. Figure 3(a) shows a typical Ohmic current−voltage (I−V) behavior at different temperatures. The Ohmic contact was made with silver paste painted at four corners of the sample in a square shape. The resistivity versus temperature for the spinel $ZnGa_2O_4$ sample is shown in figure 3(b). At 850 K, the resistivity was measured as 1.9×10^2 Ω·cm, and increased to 5.3×10^4 Ω·cm at 550 K. Hall voltage (V_H) versus magnetic field (0–1.6 T) at 700–850 K for a $ZnGa_2O_4$ sample is shown in figure 3(c),

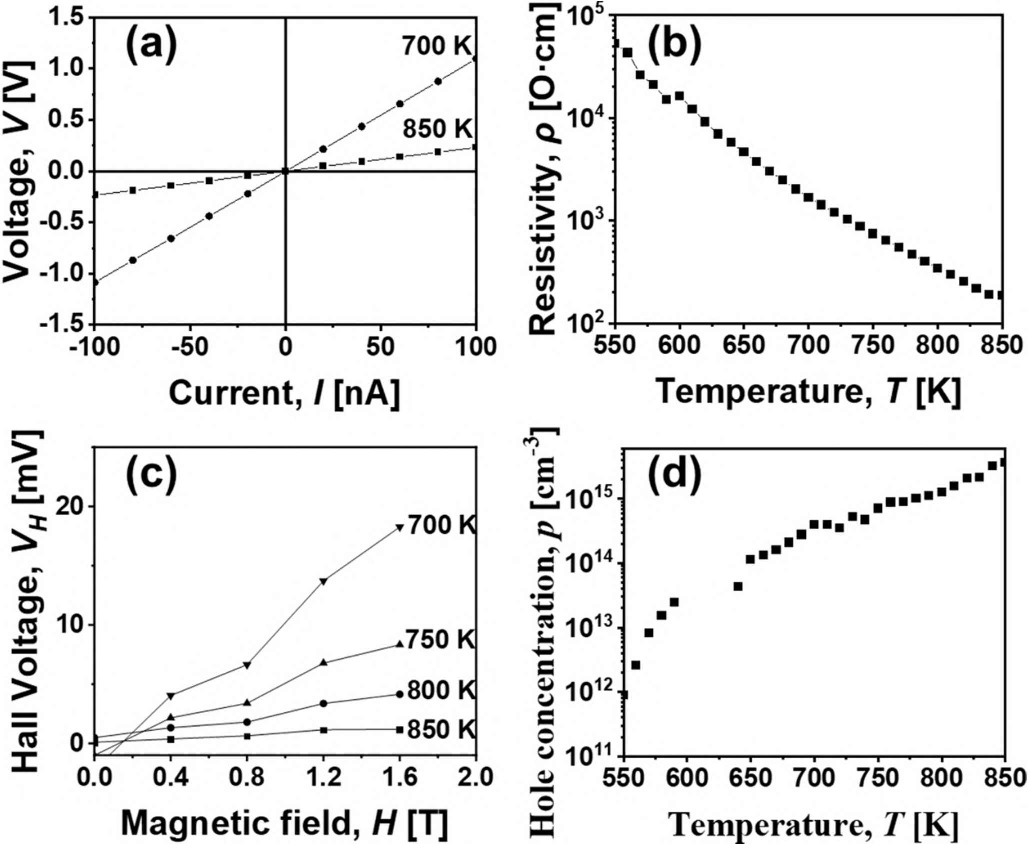

Figure 3. (a) Ohmic $I-V$ characteristics at 700 K and 850 K (b) Resistivity versus temperature. (c) Hall voltage (V_H) versus magnetic field at different temperatures (700–850 K). The Hall voltage is positive and increase with the increasing applied magnetic field, indicating the p-type conductivity in $ZnGa_2O_4$ layer. (d) Temperature dependence for Hall free hole concentration for $ZnGa_2O_4$ thin film.

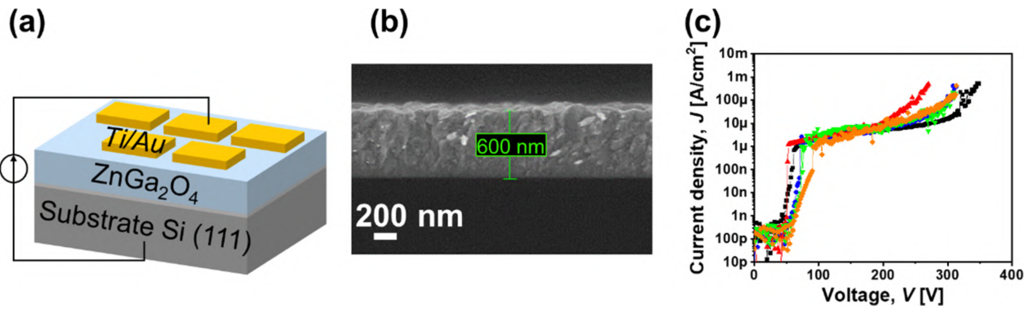

Figure 4. (a) Sketch of the vertical heterojunction structure with Ti/Au metal contacts. (b) SEM cross-section image of $ZnGa_2O_4$ polycrystalline film deposited on Si(111). The estimated thickness of the film is 600 nm. (c) Experimental $I–V$ curves of vertical breakdown voltage measurements through the $ZnGa_2O_4$/Si structure, indicating a hard breakdown voltage up to 350 V at room temperature.

the positive V_H increases with a perpendicularly applied magnetic field in a Van der Pauw configuration, which evidenced that our spinel $ZnGa_2O_4$ thin film has p-type conductivity at elevated temperature. The temperature dependence for Hall hole concentration is shown in figure 3(d) for p-type $ZnGa_2O_4$ film, the hole concentration was measured between 8.8×10^{11} and 3.7×10^{15} cm^{-3} at 550–850 K. Although the hopping behavior starts to pronounce below 600 K, extrapolating the band-activated regime of the hole concentration versus temperature at the higher temperatures, the hole density is below 10^{11} cm^{-3} at 300 K, confirming the low level of p-type doping with the applied growth conditions. The mobility of the p-type $ZnGa_2O_4$ thin film varies between 9 and 15 cm^2 (V·s)$^{-1}$.

3.4. $ZnGa_2O_4$ critical electric field

To determine the vertical critical electric field experimentally, vertical parallel plane capacitors has been fabricated by depositing Ti/Au contacts (with a size of 170 μm $\times$ 300 μm) onto p-type $ZnGa_2O_4$ grown onto the conducting Si thin films (figure 4(a)). Figure 4(b) shows the SEM cross-section image revealing that the thickness of the $ZnGa_2O_4$/Si is 600 nm.

Table 1. Comparison of various wide-bandgap semiconductor materials properties [26, 34, 35].

	4H-SiC	GaN	β-Ga_2O_3	$ZnGa_2O_4$
Crystal structure	Hexagonal (Wurtzite)	Hexagonal (Wurtzite)	Monoclinic	Cubic (Spinel)
Space group	P63mc	P63mc	C2/m	Fd-3m
Direct bandgap, E_g (eV)	3.2	3.4	4.8	4.8
Dielectric constant, ε	9.7	9	10 [36]	10.4 [37]
Critical electric field, E_{CR}(MV cm^{-1})	3.5	3.9	8[a] [24], 8.32[b], 5.7 [c], 13.2 [c] [26]	>5.3[*]
Electron mobility, μ(cm^2 (V·s)$^{-1}$)	1000	1250	300	100
Hole mobility, μ(cm^2 (V·s)$^{-1}$)	106 (300 K) [38]	34 (300 K) [39]	∼10 (high T) [26]	∼10 (high T)
Saturation velocity, v_s(10^7 cm s^{-1})	2	2.5	1.8–2	—
Thermal conductivity, λ(W (cm·K)$^{-1}$)	4.9	2.3	0.1–0.3	0.22

[*] Experimental E_{CR} values measured by authors.
[a] Common value form literature.
[b] p-NiO/n-Ga_2O_3 [25].
[c] p-Ga_2O_3 [22].

The vertical hard breakdown voltage V_{BR} was in the range of 270–350 V (figure 4(c)). It can be pointed out that a low leakage current below 1 mA mm^{-2} is observed all the way to the breakdown voltage. A thin SiO_2 layer (2 nm) at the interface $ZnGa_2O_4$/Si can often be seen [32] after the growth. To exclude the influence of the SiO_2 layer, a bare Si substrate with a native SiO_2 (2–3 nm thick layer) has been characterized as well. The vertical breakdown voltage of around 10 V [26] is considered to produce a negligible contribution to the experimentally measured V_{BR} of p-type $ZnGa_2O_4$/Si structure. Taking the experimentally determined 600 nm thickness for the $ZnGa_2O_4$ layer and extracting bare Si substrate related V_{BR} into account, the average vertical critical electric field across the film can be as high as E_{CR} 5.3 MV cm^{-1}, which is already significantly larger than the one from SiC and (single crystal) GaN. Therefore, the blank of breakdown field for $ZnGa_2O_4$ in the literature for assessing WBG semiconductors [34] can be filled as shown in table 1.

4. Conclusion

In this work, following a thermodynamic analysis, highly resistive undoped polycrystalline $ZnGa_2O_4$ thin film of 600 nm were grown on p-type silicon substrate by MOCVD. The conductivity and hole concentration of the film at 550 K were determined to be as low as 5×10^4 Ω·cm and 9×10^{11} cm^{-3}, respectively. The average breakdown voltage of $ZnGa_2O_4$/Si vertical structures was $V_{BR} = 350$ V, resulting in a critical electric field E_{CR} of 5.3 MV cm^{-1}. This value is already near twice the breakdown electrical fields of SiC and GaN and is in line with previous demonstration of its binary counterpart, Ga_2O_3. We believe that this first experimental estimation of E_{CR} for polycrystalline $ZnGa_2O_4$ will trigger further studies related to nanocrystal and high quality and homo-epitaxial films growth for future possible integration of spinel $ZnGa_2O_4$ and doped relatives for electronic and opto-electronic devices.

Data availability statement

The data cannot be made publicly available upon publication because no suitable repository exists for hosting data in this field of study. The data that support the findings of this study are available upon reasonable request from the authors.

Acknowledgments

The present work is a part of 'GALLIA' International Research Project, CNRS, France. GEMaC colleagues acknowledge financial support of French National Agency of Research (ANR), project 'GOPOWER', CE-50 N0015-01. The ICN2 is funded by the CERCA programme/Generalitat de Catalunya and by the Severo Ochoa programme of the Spanish Ministry of Economy, Industry and Competitiveness (MINECO, Grant No. SEV-2017-0706).

Conflict of interest

There are no conflicts to declare.

ORCID iDs

Zeyu Chi https://orcid.org/0000-0003-1391-527X
Ismail Madaci https://orcid.org/0000-0003-4698-0086
Ekaterine Chikoidze https://orcid.org/0000-0002-6566-4639

References

[1] Chi Z, Asher J J, Jennings M R, Chikoidze E and Pérez-Tomás A 2022 Ga_2O_3 and related ultra-wide bandgap power semiconductor oxides: new energy electronics solutions for CO_2 emission mitigation *Materials* **15** 1164
[2] Sood A, Tarntair F-G, Wang Y-X, Chang T-C, Chen Y-H, Liu P-L and Horng R-H 2021 Performance enhancement of

$ZnGa_2O_4$ Schottky type deep-ultraviolet photodetectors by oxygen supercritical fluid treatment *Results Phys.* **29** 104764
[3] Huang P-H, Shen Y-C, Tung C-Y, Huang C-Y, Tan C S and Horng R-H 2020 Energy-saving $ZnGa_2O_4$ phototransistor improved by thermal annealing *ACS Appl. Electron. Mater.* **2** 3515–21
[4] Shen Y-C, Huang P-H, Tung C-Y, Huang C-Y, Tan C-S, Huang Y-S, Chen L-J, He J-H and Horng R-H 2020 Power saving high performance deep-ultraviolet phototransistors made of $ZnGa_2O_4$ epilayers *ACS Appl. Electron. Mater.* **2** 590–6
[5] Shen Y C, Tung C Y, Huang C Y, Lin Y C, Lin Y G and Horng R H 2019 Study on optoelectronic characteristic of $ZnGa_2O_4$ thin-film phototransistors *ACS Appl. Electron. Mater.* **1** 783
[6] Tung J-C, Chiang Y-H, Wang D-Y and Liu P-L 2020 Adsorption of NO_2 and H_2S on $ZnGa_2O_4$(111) thin films: a first-principles density functional theory study *Appl. Sci.* **10** 8822
[7] Cheng L-C, Huang C-Y and Horng R-H 2018 Thickness effect on operational modes of $ZnGa_2O_4$ MOSFETs *IEEE J. Electron Devices Soc.* **6** 432–7
[8] Shen Y-C, Tung C-Y, Huang C-Y, Lin Y-C, Lin Y-G and Horng R-H 2019 Study on optoelectronic characteristics of $ZnGa_2O_4$ thin-film phototransistors *ACS Appl. Electron. Mater.* **1** 783–8
[9] Shen Y-S, Wang W-K and Horng R-H 2017 Characterizations of metal-oxide-semiconductor field-effect transistors of ZnGaO grown on sapphire substrate *IEEE J. Electron Devices Soc.* **5** 112–6
[10] Castaing V, Giordano L, Richard C, Gourier D, Allix M and Viana B 2021 Photochromism and persistent luminescence in Ni-doped $ZnGa_2O_4$ transparent glass-ceramics: toward optical memory applications *J. Phys. Chem.* C **125** 10110–20
[11] Paudel T R, Zakutayev A, Lany S, d'Avezac M and Zunger A 2011 Doping rules and doping prototypes in A_2BO_4 spinel oxides *Adv. Funct. Mater.* **21** 4493–501
[12] Shi Y *et al* 2014 Self-doping and electrical conductivity in spinel oxides: experimental validation of doping rules *Chem. Mater.* **26** 1867–73
[13] Look D C, Leedy K D, Horng R-H, Santia M D and Badescu S C 2020 Electrical and optical properties of degenerate and semi-insulating $ZnGa_2O_4$: electron/phonon scattering elucidated by quantum magnetoconductivity *Appl. Phys. Lett.* **116** 252104
[14] Chikoidze E *et al* 2020 p-type ultrawide-band-gap spinel $ZnGa_2O_4$: new perspectives for energy electronics *Cryst. Growth Des.* **20** 2535–46
[15] Chi Z *et al* 2021 Bipolar self-doping in ultra-wide bandgap spinel $ZnGa_2O_4$ *Mater. Today Phys.* **20** 100466
[16] Sabino F P, Chatratin I, Janotti A and Dalpian G M 2022 Hole conductivity through a defect band in ZnG_a2O_4 *Phys. Rev. Mater.* **6** 064602
[17] Liu J *et al* 2022 Pt/$ZnGa_2O_4$ Schottky barrier diodes fabricated by using single crystal n-$ZnGa_2O_4$ (111) Substrates *IEEE Electron Device Lett.* **43** 2061–4
[18] Baliga B J 1989 Power semiconductor device figure of merit for high-frequency applications *IEEE Electron Device Lett.* **10** 455–7
[19] Trew R J 1997 Experimental and simulated results of SiC microwave power MESFETs *Phys. Status Solidi* a **162** 409–19
[20] Fischer A J, Dickerson J R, Armstrong A M, Moseley M W, Crawford M H, King M P, Allerman A A, Kaplar R J, van Heukelom M S and Wierer J J 2016 High voltage and high current density vertical GaN power diodes *Electron. Lett.* **52** 1170–1
[21] Allerman A A, Armstrong A M, Fischer A J, Dickerson J R, Crawford M H, King M P, Moseley M W, Wierer J J and Kaplar R J 2016 Al0.3Ga0.7N PN diode with breakdown voltage >1600 V *Electron. Lett.* **52** 1319–21
[22] Chu T L and Kelm R W 1975 The preparation and properties of aluminum nitride films *J. Electrochem. Soc.* **122** 995
[23] Wort C J H and Balmer R S 2008 Diamond as an electronic material *Mater. Today* **11** 22–28
[24] Higashiwaki M, Sasaki K, Kuramata A, Masui T and Yamakoshi S 2012 Gallium oxide (Ga_2O_3) metal-semiconductor field-effect transistors on single-crystal β-Ga_2O_3 (010) substrates *Appl. Phys. Lett.* **100** 013504
[25] Zhang J *et al* 2022 Ultra-wide bandgap semiconductor Ga_2O_3 power diodes *Nat. Commun.* **13** 3900
[26] Chikoidze E *et al* 2020 Ultra-high critical electric field of 13.2 MV/cm for Zn-doped *p*-type β-Ga_2O_3 *Mater. Today Phys.* **15** 100263
[27] Kroger F A 1964 *The Chemistry of Imperfect Crystals* (New York: Wiley)
[28] Galazka Z *et al* 2019 Ultra-wide bandgap, conductive, high mobility, and high quality melt-grown bulk $ZnGa_2O_4$ single crystals *APL Mater.* **7** 022512
[29] Yu Z, Yang Y and Sun J 2021 Electroluminescence from Er-doped $ZnGa_2O_4$ spinel nanofilms fabricated by atomic layer deposition on silicon *Opt. Mater.* **122** 111691
[30] Horng R-H, Huang C-Y, Ou S-L, Juang T-K and Liu P-L 2017 Epitaxial growth of $ZnGa_2O_4$: a new, deep ultraviolet semiconductor candidate *Cryst. Growth Des.* **17** 6071–8
[31] Wang W-K, Liu K-F, Tsai P-C, Xu Y-J and Huang S-Y 2019 Influence of annealing temperature on the properties of $ZnGa_2O_4$ thin films by magnetron sputtering *Coatings* **9** 859
[32] Wang W-K, Xu Y-J, Huang L and Tsai P C 2019 Structural characteristics and photoluminescence properties of sputter-deposition $ZnGa_2O_4$ thin films on sapphire and Si(100) Substrates *Coatings* **9** 469
[33] Yi S S, Kim I W, Park H L, Bae J S, Moon B K and Jeong J H 2003 Luminescence characteristics of pulsed laser deposited $ZnGa_2O_4$ thin film phosphors grown on various substrates *J. Cryst. Growth* **247** 213–8
[34] Chen M-I, Singh A K, Chiang J-L, Horng R-H and Wuu D-S 2020 Zinc gallium oxide—a review from synthesis to applications *Nanomaterials* **10** 2208
[35] Pearton S J, Yang J, Cary P H, Ren F, Kim J, Tadjer M J and Mastro M A 2018 A review of Ga_2O_3 materials, processing, and devices *Appl. Phys. Rev.* **5** 011301
[36] Passlack M, Hunt N E J, Schubert E F, Zydzik G J, Hong M, Mannaerts J P, Opila R L and Fischer R J 1994 Dielectric properties of electron-beam deposited Ga_2O_3 films *Appl. Phys. Lett.* **64** 2715–7
[37] Xue J, Wu S and Li J 2013 Synthesis, microstructure, and microwave dielectric properties of spinel $ZnGa_2O_4$ ceramics ed N Alford *J. Am. Ceram. Soc.* **96** 2481–5
[38] Arakawa Y, Ueno K, Kobayashi A, Ohta J and Fujioka H 2016 High hole mobility p-type GaN with low residual hydrogen concentration prepared by pulsed sputtering *APL Mater.* **4** 086103
[39] Matsuura H, Komeda M, Kagamihara S, Iwata H, Ishihara R, Hatakeyama T, Watanabe T, Kojima K, Shinohe T and Arai K 2004 Dependence of acceptor levels and hole mobility on acceptor density and temperature in Al-doped p-type 4H-SiC epilayers *J. Appl. Phys.* **96** 2708–15